

Article

An Evaluation Model for Analyzing Robustness and Spatial Closeness of 3D Indoor Evacuation Networks

Lei Niu ^{1,*}, Zhiyong Wang ² , Yiquan Song ³ and Yi Li ⁴

¹ Faculty of Geomatics, Lanzhou Jiaotong University, Lanzhou 730070, China

² Human Geography and Spatial Planning, Utrecht University, 3584 CB Utrecht, The Netherlands; z.wang2@uu.nl

³ School of Geographic and Environmental Sciences, Tianjin Normal University, Tianjin 300387, China; songyiquan@tjnu.edu.cn

⁴ Institute of Remote Sensing and Digital Earth, Chinese Academy of Sciences, Beijing 100094, China; liyi@radi.ac.cn

* Correspondence: l.niu@lzjtu.edu.cn

Abstract: Indoor evacuation efficiency heavily relies on the connectivity status of navigation networks. During disastrous situations, the spreading of hazards (e.g., fires, plumes) significantly influences indoor navigation networks' status. Nevertheless, current research concentrates on utilizing classical statistical methods to analyze this status and lacks the flexibility to evaluate the increasingly disastrous scope's influence. We propose an evaluation method combining 3D spatial geometric distance and topology for emergency evacuations to address this issue. Within this method, we offer a set of indices to describe the nodes' status and the entire network under emergencies. These indices can help emergency responders quickly identify vulnerable nodes and areas in the network, facilitating the generation of evacuation plans and improving evacuation efficiency. We apply this method to analyze the fire evacuation efficiency and resilience of two experiment buildings' indoor networks. Experimental results show a strong influence on the network's spatial connectivity on the evacuation efficiency under disaster situations.

Keywords: 3D; indoor evacuation network; spatial influence; robustness; isolation



Citation: Niu, L.; Wang, Z.; Song, Y.; Li, Y. An Evaluation Model for Analyzing Robustness and Spatial Closeness of 3D Indoor Evacuation Networks. *ISPRS Int. J. Geo-Inf.* **2021**, *10*, 331. <https://doi.org/10.3390/ijgi10050331>

Academic Editors: Eliseo Clementini and Wolfgang Kainz

Received: 8 March 2021

Accepted: 4 April 2021

Published: 13 May 2021

Publisher's Note: MDPI stays neutral with regard to jurisdictional claims in published maps and institutional affiliations.



Copyright: © 2021 by the authors. Licensee MDPI, Basel, Switzerland. This article is an open access article distributed under the terms and conditions of the Creative Commons Attribution (CC BY) license (<https://creativecommons.org/licenses/by/4.0/>).

1. Introduction

Emergency evacuation is a process in which people in dangerous areas have to be guided or transported to safe places. It plays an essential part in crisis management, saving people's lives and property. Since the occurrences of some notable emergency events, such as terrorist attacks on 11 September 2001 and the 2005 London bombing (which occurred in indoor environments), increased attention has been paid to indoor emergency evacuation [1–4]. We could classify the practical usages of this type of research into three categories: (1) to optimize the spatial designs of indoor environments; (2) to improve the configurations of the emergency response facilitates (exit lights, fire hose) for firefighting; (3) to assist with generating evaluation plans.

Indoor emergency evacuation is a complex phenomenon influenced by many factors, such as human awareness and interactions, hazard spread, and indoor environments. With the increased interest in indoor emergencies in recent years, many researchers have conducted studies to study the influences of these factors on evacuation efficiency in indoor environments during emergencies. The authors of [2] proposed an agent simulation model that combines human behaviors to predict the spatial accessibility of a specific building under fire disaster situations. The authors of [1] combined 3D spatial neighboring with topological relationships to implement a CA-based building evacuation simulation system. In [3], the authors applied a multigrid model to study the pedestrian evacuation process under blind conditions and discovered several critical characteristics of the evacuees. The study in [5] checked potential bioterrorism attacks on subway stations and

inspected the influences of hazardous materials on the evacuees. However, the studies mentioned above mainly focused on human behaviors and interactions during evacuations. To the best of our knowledge, few works have evaluated spatial units' connectivity in 3D environments for indoor emergency evacuation.

2. Related Works

An important aspect related to indoor emergency evacuation is navigation. During emergencies, various obstacles (e.g., fires, floods, and plumes) can affect road networks, and people in dangerous places need guidance to reach safe areas [6]. Unlike outdoor navigation, indoor navigation occurs in 3D spaces and requires both the topological and geometric 3D information of route planning environments. Many efforts have shed light on developing models and methods for the efficient representation of 3D data for indoor navigation purposes [7–11]. In recent decades, with the increased attention paid to indoor emergencies, many researchers have directed their interests to indoor navigation in disastrous situations and have developed new models and methods to support routing in indoor environments. The studies in [12–15] systematically exploited a 3D graph network model integrated with the metric distance measure to help emergency responders and evacuees determine the safest egress paths quickly. The authors of [16] fully applied a three-dimensional geometric network to compute evacuation routes for evacuees and generated two types of “almost-optimal” and “almost feasible” solutions considering time constraints. However, these above works only addressed route generation in different disaster situations, and few researchers have paid attention to analyzing the robustness of networks affected by hazards. Because 3D networks play a major role in the generation of indoor routes, there is also a need to analyze the indoor routing network under study's status to facilitate route calculations during emergencies.

Network representations have been used in various fields to model real-world problems, such as social networks, traffic networks, and power networks. Researchers have developed a rich set of methods to address these problems and analyze networks for various purposes [17,18]. The authors of [19] proposed multiple centrality assessment systems to evaluate the nature of a network from a primal perspective. This system can show the metric distances and other indices of the centrality features of the studied graphs. For general cases regarding network connectivity statuses, References [20,21] explored some essential characteristics and dynamics for urban street network gridlocks and developed a model to reproduce hysteresis and network gridlocks. They applied the developed model to significant city networks and discovered some phenomena from the whole network's perspective. In [22], the authors proposed a robustness analysis model based on short-term variations in supplies. This model is efficient for demonstrating the vulnerabilities of specific networks. In [23], the authors conducted a systematic structural vulnerability analysis for a large-scale power grid structure according to complex network principles. This model can identify the vulnerable spots in a network. The authors of [24–26] studied the community structures existing in several large networks and the influences of their effects during random and infectious attacks. In [27,28], the authors investigated the impacts of illness carriers among a complex network and found that the most influential spreaders are the nodes that have the highest k -decomposition values instead of the considerable connectivity values suggested by the classical evaluation methods. Although these existing network studies have provided insights into navigation networks' evaluation from a topological aspect, they lack consideration for 3D geometric information, limiting their applicability concerning the analysis of indoor navigation networks.

In this study, we investigate the evaluation of networks for indoor emergencies and propose a method to analyze networks' robustness under emergencies. In this method, we use the 3D spatial distance as the edge weight for the generation of navigation paths and consider both the network topology and 3D spatial distance in the network analysis. The 3D spatial distance usage allows us to evaluate the given 3D network more realistically and holistically. Furthermore, we introduce hazard models to evaluate the connectivity status

of the indoor network. Thus, by integrating hazard models, we can estimate the influence of hazards on the network structure over time (i.e., by dynamically dividing the main network into isolated subnetworks) and update the weights of edges in the indoor navigation network. We propose a set of indices for the evaluation of nodes and the whole network. These indices can help us examine the network's status in a 3D environment affected by hazards and identify vulnerable nodes and edges, facilitating the generation of evacuation plans for indoor emergencies. We organize the rest of this paper as follows: in Section 3.1, we present the indices proposed for the connectivity analysis of 3D indoor navigation networks. In Sections 3.2–3.4, we take a fire event as an example and present our method to study the isolation phenomena of an indoor network affected by fires. In these sections, we carry out experiments and test our method with two buildings' datasets. Section 3.5 describes our experiments and Section 4 presents the experiments results. Finally, in Section 5, we provide our conclusions and suggest future research directions.

In the next part, we present a set of indices that define network connectivity at the global and local levels. At the global level, we use selected indices to examine the connection efficiency of the entire network. We evaluate the connection effectiveness for the neighborhood of specifically studied graphs and estimate the local influences of the considered neighboring nodes or edges at the local level. The developed indices use nodes as fundamental elements for examining purposes and integrating spatial correlations with nearby objects to describe the same spatial characteristics in the indoor navigation network. We generally elaborate on the classical indices that play the function of measuring the graph statuses below:

A. Gamma index

The gamma index is a measure of connectivity that considers the relationship between the number of observed links and possible links. The value of gamma is between 0 and 1, where a value of 1 indicates a completely connected network, which would be extremely unlikely in reality. We use this index to measure the progression of a network over time.

B. General transitivity

Transitivity is the overall probability of having its adjacent nodes be interconnected, thus revealing tightly connected communities. We use the measure of general transitivity that is calculated by the average clustering coefficient for all nodes.

C. Average node path length

The average shortest path length is a measure of efficiency representing the average number of steps needed to reach two distant nodes in the graph. The lower the result is, the more efficient the network in providing ease of circulation. In this paper, we use a node as the unit of measuring the average path length.

D. Graph diameter

The graph diameter is the length of the shortest path between the most distanced nodes of a graph. It measures the extent of a graph and the topological length between two nodes.

E. Local connectivity

Connectivity is the minimum number of deletion elements to separate the remaining nodes into isolated sub-graphs. We introduce the concept of local connectivity generated by the arithmetic mean of all nodes' connectivity values.

3. Research Methodology

3.1. The Proposed Method

In the following part, we show the six indices definitions of the proposed method for network evaluation. The first index is the clustering coefficient and an indicator for describing the spatial influence of removing a specific node in the network. The second index is the average cost of local neighbor node counts and depicts the number of neighboring nodes of a specific node covered by the ordinary node distance scope. The third index

is the 3D spatial distance, which describes a neighboring node's spatial closeness from a specific node, and so it is a spatial influence indicator for this source node. The fourth index is the meaningful result count used to depict the mean count for the generated path result. The path results mentioned in this paper are all generated by the Dijkstra algorithm. The fifth index is the average time cost of pathfinding and describes the general case of the time cost spent on the pathfinding process. The last index is the average length of the path used to demonstrate the general distances of output paths; two sub-indices implement it: the average path lengths measured by the node distance and spatial distance. Moreover, in Equations (1)–(9), we use the symbol v to represent a specific node; the symbol e to represent an edge; the symbol V to represent the complete node set; and the symbols p and P to represent the generated path and complete path set in the corresponding graph, respectively. Table 1 summarizes the index symbols used in this paper.

Table 1. Index symbols of the proposed method.

Symbol	Meaning
v	the current considering node
V	the complete node set
V_i	the node i 's neighboring node set
e_{uw}	the edge collection formed by nodes u and w in the set V_i
$u w$	the nodes other than the considering node
E	the complete edge set
$ e $	the edge e 's length
k_v	the size of the set V_i
n	the number of considering nodes
SD_{vw}	the spatial distance between selected nodes v and w
Q	the total average number of nodes outside the SD scope
SD	the average spatial distance between all selected nodes
Q_v	the number of nodes outside the SD scope for the considering node
C_v	the regional connectivity index for the specific node
C_l	the average regional connectivity index of all nodes
T_{aop}	the average time cost of successfully generating evacuation paths
T_p	the average time cost of a specific generated evacuation path
N_p	the node number of a specific evacuation path
p	the current evacuation path of the considering node
P	the complete evacuation path set
t	the time cost of generating an evacuation path
C_r	the meaningful result count for a specific test successfully generating evacuation paths
C_m	the average meaningful result count of all tests successfully generating evacuation paths
C_{zero}	the zero set of the meaningful result count for tests unsuccessfully generating evacuation paths
C_{null}	the null set of the meaningful result count for tests unsuccessfully generating evacuation paths
I	the node number of the complete node set
L_{aop}	the average length of generated evacuation paths
L_p	the length for a specific generated evacuation path
ND_p	the average node distance of generated evacuation paths
$ND_{v_i v_{i-1}}$	the node distance between two nodes v_i and v_{i-1}
SD_p	the average spatial distance of generated evacuation paths
$SD_{v_i v_{i-1}}$	the spatial distance between two nodes v_i and v_{i-1}

A. Node clustering coefficient

Equation (1) produces the clustering coefficient for a specific node v . To compute this index, we first calculate the number of edges in node v 's neighboring node-set V_i after the deletion of node v from the navigation network. e_{uw} represents the edge collection formed by nodes u and w in the set V_i . k_v is the size of set V_i , which equals the number of nodes in this set. This index illustrates the influence of a selected node on the entire

navigation network. Since this index's value represents the importance of the considered node in the system, a larger value means that this node's deletion would have a lesser impact on the system's passing efficiency.

$$C_v = \frac{|\{e_{uw} : u, w \in V_i, e_{uw} \in E\}|}{k_v(k_v - 1)/2} \quad (1)$$

B. The average cost of the local connectivity index

When calculating the average cost of the regional connectivity index for all nodes in the network, we aim to measure the node deletion process's average influence level in the system. This value indicates a general perspective of the neighborhood clustering status in Equation (2).

$$C_l = \frac{1}{n} \sum_{v \in V} (C_v) \quad (2)$$

C. 3D spatial distance and spatial closeness of a neighboring node

Aiming to demonstrate the considered navigation network's 3D spatial distribution, we introduce two coefficients generated by Equations (3) and (4). In Equation (3), SD_{vw} represents the 3D distance between any two connected nodes v and w in the navigation network, and $|e|$ represents the number of edges in the same system. The average spatial distance cost of edge SD shows the mean travel distance for existing edges. Currently, these edges are undirected; we will consider directed edges in future work.

$$SD = \frac{1}{|e|} \sum_{v, w \in V, v \neq w} SD_{vw} \quad (3)$$

Equation (4) generates a quantitative index Q for illustrating the spatial closeness of neighboring nodes in the navigation network, and two steps accomplish the computation of this index computation. The first step computes the number of nodes spread in the spatial scope around the considered node v . In detail, this scope is a 3D ball formed by using the 3D coordinates of v as the center and the value generated by Equation (3) as the radius SD . In other words, there are the nodes with spatial distances SD_{vw} smaller than SD , where w represents any neighboring node of the current considered node v . After setting up covering balls, we generate an adjacent set of Q_v that contains every ball's covering nodes. Then, in the second step, we calculate the arithmetic mean Q for the entire navigation network with the previously defined Q_v values for all nodes by dividing this sum by the total node number n .

$$Q = \frac{1}{n} \sum_{v, w \in V, v \neq w, SD_{vw} < SD} (Q_v) \quad (4)$$

D. Meaningful result count

Let us first define a result count C_r that originates from calculating the meaningful evacuation paths passing a specific node marked with the label t . Therefore, the meaningful result counts, C_m , equals the sum of elements C_r neither in the zero nor null set ($C_{zero} \cup C_{null}$) that either cover the case of the considered node as the evacuation target or the case in which there is no accessible, safe evacuation path to the target node. Moreover, these values mostly come from a test that cannot generate any meaningful evacuation path or exceeds each path generation process's time threshold.

$$C_m = \sum_{t \notin (C_{zero} \cup C_{null})} (C_r) \quad (5)$$

E. The average time cost of path finding

The average time cost T_{aop} of pathfinding is the mean value among every specific type of path generating principle for the compared methods. Moreover, it is the average sum (generated by subdividing the path node number N_p) of the time cost T_p for each path p in the complete evacuation path set P .

$$T_{aop} = \frac{1}{N_p} \sum_{p \in P} (T_p) \quad (6)$$

F. Average length of generated paths

The average length of path finding L_{aop} is the average value (generated by subdividing the path node number N_p) of the generated path distance L_p for each successfully generated path p in the complete path search set P . This value is introduced to reflect the effect of applying different optimization principles for our solution. For each path $p = \{v_1, \dots, v_i, v_{i+1}, \dots, v_I\}$, $p \in P$, I is the number of nodes along path p , and we use two distance types: the node distance and spatial distance; thus, the following two subsections describe these two distances for the average length of a path in detail.

$$L_{aop} = \frac{1}{N_p} \sum_{p \in P} (L_p) \quad (7)$$

1. The node distance ND_p is the count $ND_{v_i v_{i-1}}$ of every successive node pair along a path and is measured in counts (Equation (8)). Moreover, it reflects how the generated evacuation path traverses many critical nodes. Here, v_i denotes a node in the complete node set I for the generated path p .

$$ND_p = \sum_{i=2}^I ND_{v_i v_{i-1}} \quad (8)$$

2. The spatial distance SD_p is the sum of the spatial distances $SD_{v_i v_{i-1}}$ of every two successive nodes along a path measured in meters (Equation (9)). It shows the geometric space that is covered by the generated evacuation path. Here, v_i denotes a node of the complete node set I for the generated path p .

$$SD_p = \sum_{i=2}^I SD_{v_i v_{i-1}} \quad (9)$$

3.2. Isolation Study and Recovery of the Spatial Navigation Network for a Spreading Fire

Unlike the static environments of typical navigation situations, evacuation navigation must take the dynamics of the spreading hazards into account. As a threat develops, many edges and nodes in the navigation network become affected and unavailable. This situation can deteriorate when the threats block all main egresses. Under this circumstance, many isolated subnetworks can emerge due to their egress routes becoming blocked, and we call this situation the isolation of the navigation network.

The isolation phenomenon can significantly hinder evacuation efficiency, and under extreme situations, it can even paralyze the entire evacuation network due to the unavailability of all safe egress routes. Nevertheless, emergency responders can apply ladders or personnel lowering devices to construct new egress paths. Therefore, the resilience of the navigation network for evacuation purposes is also crucial. From our perspective, we can split fire disasters' primary development process into three phases: the ignition phase, the entire development phase, and the egress closure phase. These phases have different spatial influences on the navigation network. In the first phase, only the fire source and its nearby surrounding region are inaccessible. In the second phase, fire development is severe, and it paralyzes a large part of the navigation network. In the final stage, hazards

block most critical nodes in the navigation network, and no safe egress paths are available. We are currently only considering a particular ignition position and carefully studying the multiple ignition positions in future work. Furthermore, we would also conclude the difference of the fire resistance features of various building and furniture materials, for example, plastic, wood, and paint, in future research on the fire spreading models.

3.3. Estimation of the Spread of Fire in a 3D Navigation Network

As previously mentioned, the spread of a fire has a spatial influence on the navigation network. We can describe this process by marking the passage statuses of nodes covered by the hazard, such as transit areas filled with fire plumes and flames, as blocked. Therefore, a fire model must estimate fires' spatial influence on the navigation network and obtain information about the building's navigation conditions during disasters.

In this study, we use a fire model (Equation (10)) to estimate the fire's spatial influence during the full development phase. In this equation, x_0 , y_0 , and z_0 represent the fire source's initial coordinates; s_x , s_y , and s_z represent the speed of the spread of the developing fire across three axes. t_0 represents the starting time of the current phase, and t represents the present time. x_{min} and x_{max} represent the current minimum and maximum coverage of the fire along the X-axis. The same explanation also applies to y_{min} and y_{max} for the Y-axis and z_{min} and z_{max} for the Z-axis. Here, t represents the development time for the fire event.

$$\begin{cases} x_{min} = x_0 - s_x \times (t - t_0) \\ x_{max} = x_0 + s_x \times (t - t_0) \\ y_{min} = y_0 - s_y \times (t - t_0) \\ y_{max} = y_0 + s_y \times (t - t_0) \\ z_{min} = z_0 - s_z \times (t - t_0) \\ z_{max} = z_0 + s_z \times (t - t_0) \end{cases} \quad (10)$$

3.4. Pre-Measures for the Recovery Analysis of an Indoor Navigation Network

As discussed at the beginning of Section 3, the spread of a disaster can reorganize the original navigation network. This phenomenon can demonstrate the isolation between several nodes and their neighbors due to the blockage of their connecting edges by hazards. This situation can result in two critical issues affecting navigation operations. The first issue is to find the minimum influence paths between these nodes, which are generated by checking the L_{oop} values from Section 2 and are named as *isolated subnetworks*. The second issue is to use the smallest number of nodes possible to address the dynamically deteriorating navigation network. To address these two issues, we rely on the spatial sorting of nodes across both the primary and isolated subnetworks, and these nodes are the same as the nodes in the building structure's skeletal framework. We have not discussed furniture, fixtures, and equipment (FF&E) in the current research stage due to the lack of reliable data for these objects. Moreover, according to the sorting results, only some sorted nodes are introduced to generate minimum influence paths across the navigation network.

3.4.1. Spatial Sorting of Nodes

We can choose different principles for sorting nodes, such as sorting them by their node distances to the fire region or their spatial distances to the fire region and applying them in this study. In our opinion, the most critical issue for evacuation navigation is to determine the effect of the 3D spatial distance weights on the network. Therefore, we set different groups of nodes by evaluating the node distances to the fire region and the fire region's spatial distances. We demonstrate this concept in Figure 1. There are 26 nodes to search for the emergency evacuation solutions in this figure. We optimize the evacuation searching process by assigning different priorities to the 22 nodes (the 4 nodes in isolated-region 1 are filtered out due to disaster coverage), as shown in Table 2. Next, we take nodes C and F as examples to explain the sorting principle. Because node C connects isolated region 1 with the minimum depth 1 to node J, the 'node distance' for node C from isolated

region 1 is 1. Following this principle, node F's 'node distance' is also 1 for isolated regions 1 and 3. Therefore, we can receive the sorted region S1' composed of nodes C, F, G, H, and I. We can finally generate three sorted regions: S1, S3, and S5, with node distances of 1 to the isolated-region 1. Thus, we select these regions with higher priorities than those of other sorted regions with node distances larger than 1 to isolated-region 1 in Figure 2.

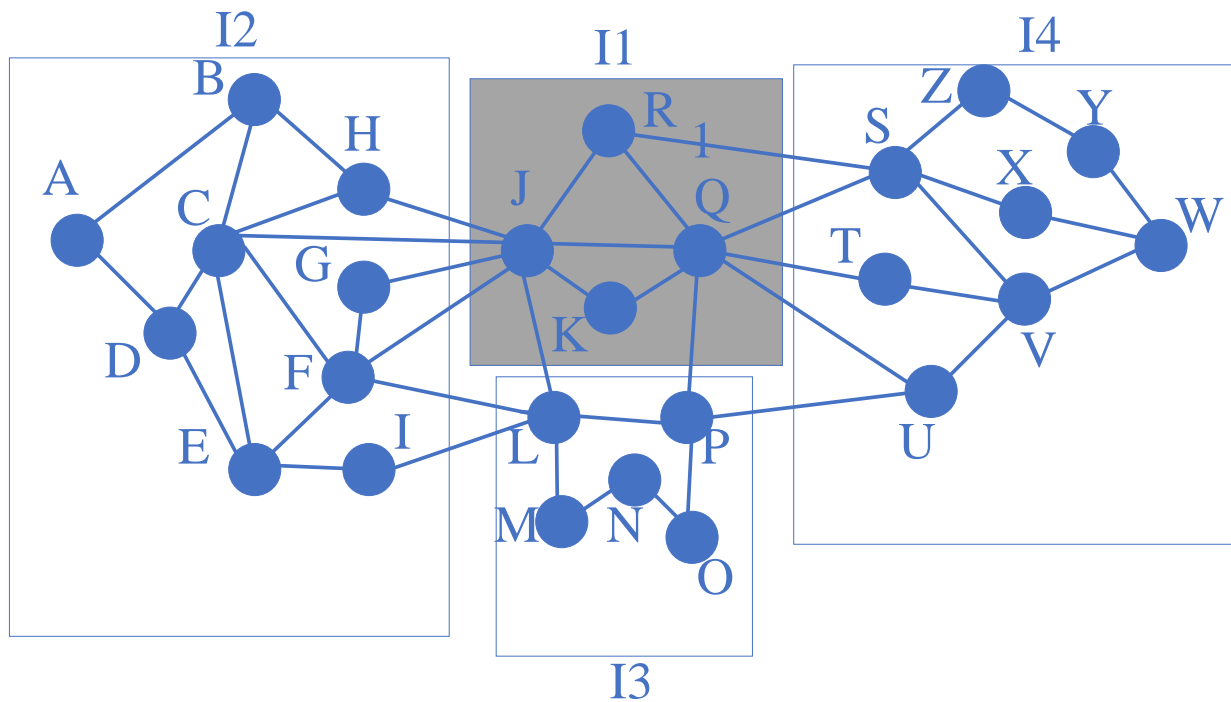


Figure 1. An example of spatial grouping mechanism for an evacuation network.

Table 2. Index and attribute value of the navigation graphs for the experiment buildings.

Node	Belong to Isolated Subnetwork	Node Distance	Connect with Subnetwork	Sorted-Region
C	I2	1	I1	S1
F	I2	1	I1,I3	S1
G	I2	1	I1	S1
H	I2	1	I1	S1
I	I2	1	I3	S1
A	I2	2	Empty set	S2
B	I2	2	Empty set	S2
D	I2	3	Empty set	S2
E	I2	2	Empty set	S2
L	I3	1	I1,I2	S3
P	I3	1	I1,I4	S3
M	I3	2	I1,I3	S4
N	I3	3	I1	S4
O	I3	2	I1	S4
S	I4	1	I1	S5
T	I4	1	I1	S5
U	I4	1	I1,3	S5
V	I4	2	Empty set	S6
W	I4	3	Empty set	S6
X	I4	2	Empty set	S6
Y	I4	3	Empty set	S6
Z	I4	2	Empty set	S6

3.4.2. Partial Selection of Nodes for Path Finding

For the spatial sorting of nodes, we arrange the sequence of nodes by a specific standard, such as the node distance to the fire region, and we fetch only the nodes relevant to the pathfinding process. For this purpose, we utilize the first 20% of the sorted nodes for evacuation path generation according to the Pareto principle [29]. Additionally, we introduce the 10%, 50%, and 80% cases of all nodes as the comparison group. The purpose of using a different number of nodes during navigation is to balance the volume of node data and the accuracy of the generated evacuation paths. When the number of nodes is extensive, using all nodes in the evacuation path generation is not optimal for saving time. Using the necessary number of nodes for the required computation is a wiser option. To this end, we can only select the exact number of nodes by fully understanding which of the nodes are crucial during evacuation path generation operations.

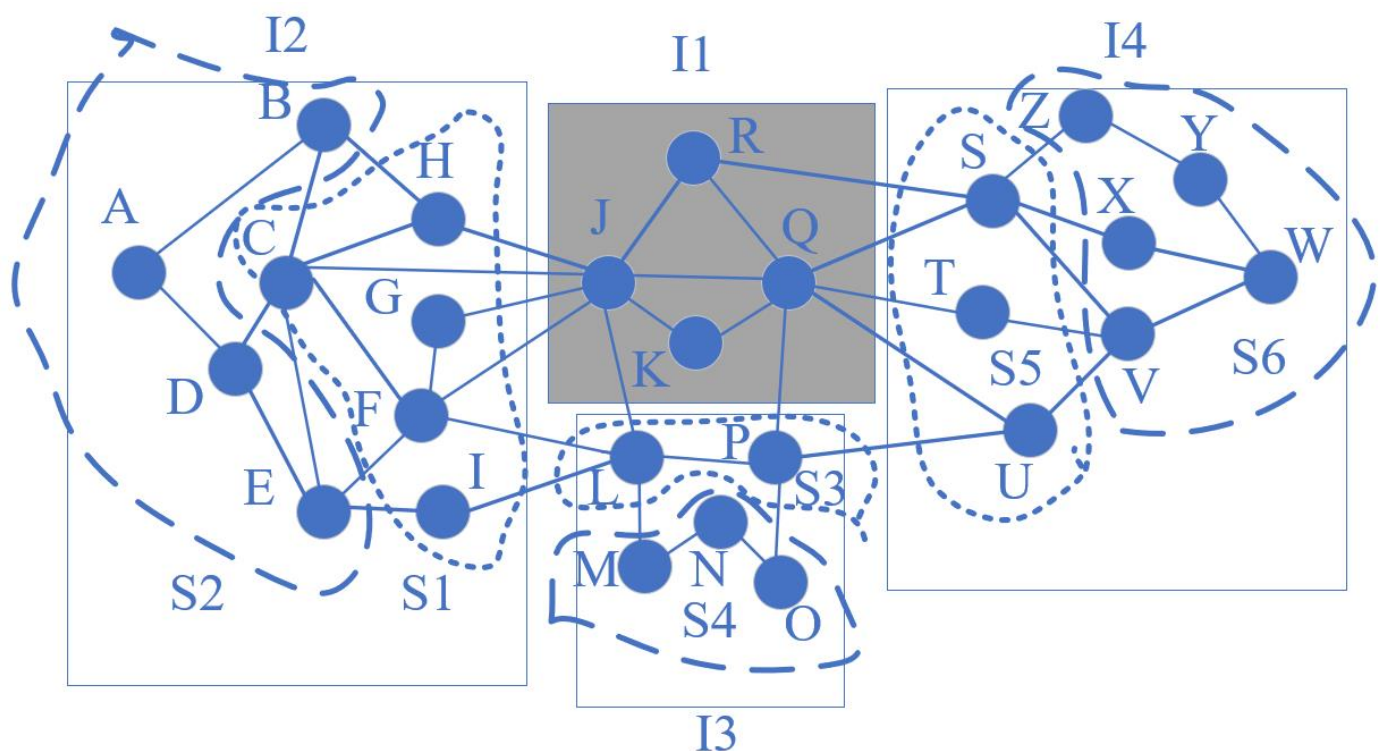


Figure 2. An example of spatial grouping result for an evacuation network. The dotted lines indicate the isolated networks that are directly influenced by the fire in I1 (in gray); the dashed lines indicate the isolated networks that will be potentially influenced by the fire in I1 (in gray).

3.5. Introduction of the Studied Buildings

We evaluate our method with the datasets of two buildings. The first is a building at the Henan University of Urban Construction (HUUC) (Figure 3). The other one is the Meiluocheng (MLC) building (Figure 4). The first building is located on Longxiang Road, Xincheng District, Pingdingshan, China, and comprises three sub-buildings, named parts A, B, and C (part A in the north, part B in the middle, and part C in the south). All three parts are connected by corridors distributed along the west and east wings. The HUUC building has four floors and is currently the primary teaching and research facility occupied by the school of surveying and urban spatial information. Therefore, evaluating this building's navigation network connectivity can reduce the risk of losing a life when facing fire events. The MLC building is on Zhaojiabang Road in Xuhui District, Shanghai, China; it has eight floors in the main structure and is famous for its giant glass ball, a landmark of Shanghai City.

First, we establish the two test buildings' graphs by applying middle axis extraction and key node extraction to the doors, corners, and stairs. Next, we set the fire sources with the following settings: we place the fire source at one node at a time and traverse the entire navigation network after all simulations, and the initial phase for the fire emergency is phase 2. In this phase, the accessibility of the neighbor nodes within a specific range of the fire source is disabled. We set this scope with parameters defined in the SFPE handbook [30] under normal fire spreading conditions: the fire-affected areas increase with a speed of 0.0015 m/s for 280 s and with a developing rate of 0.30 m/s for 140 s. The exit nodes for the MLC building are nodes 1111, 111,122, 111,164, 111,155, and 111,158. The exit nodes for the HUUC building are nodes 15, 16, 22, 25, 26, and 37.

As demonstrated in Figure 5, the navigation graph of the HUUC building clearly shows its four-layer distribution and three-part spatial division. Additionally, we can observe that part A contains many small spatial subdivisions, part B has the most intensive spatial connections among the three parts, and part C has the largest span of distributed objects. We can explain this spatial phenomenon as follows: part A contains many mid-sized classrooms for fewer than 50 students to use. Part B has many school offices, staff conference rooms, bathrooms, and two lecture halls. From Figure 6, we can see that the MLC building has two main groups of navigation nodes and another group to connect them. Additionally, due to the fire safety code, many egress routes lie around these groups of nodes to quickly evacuate customers and employees during emergencies.

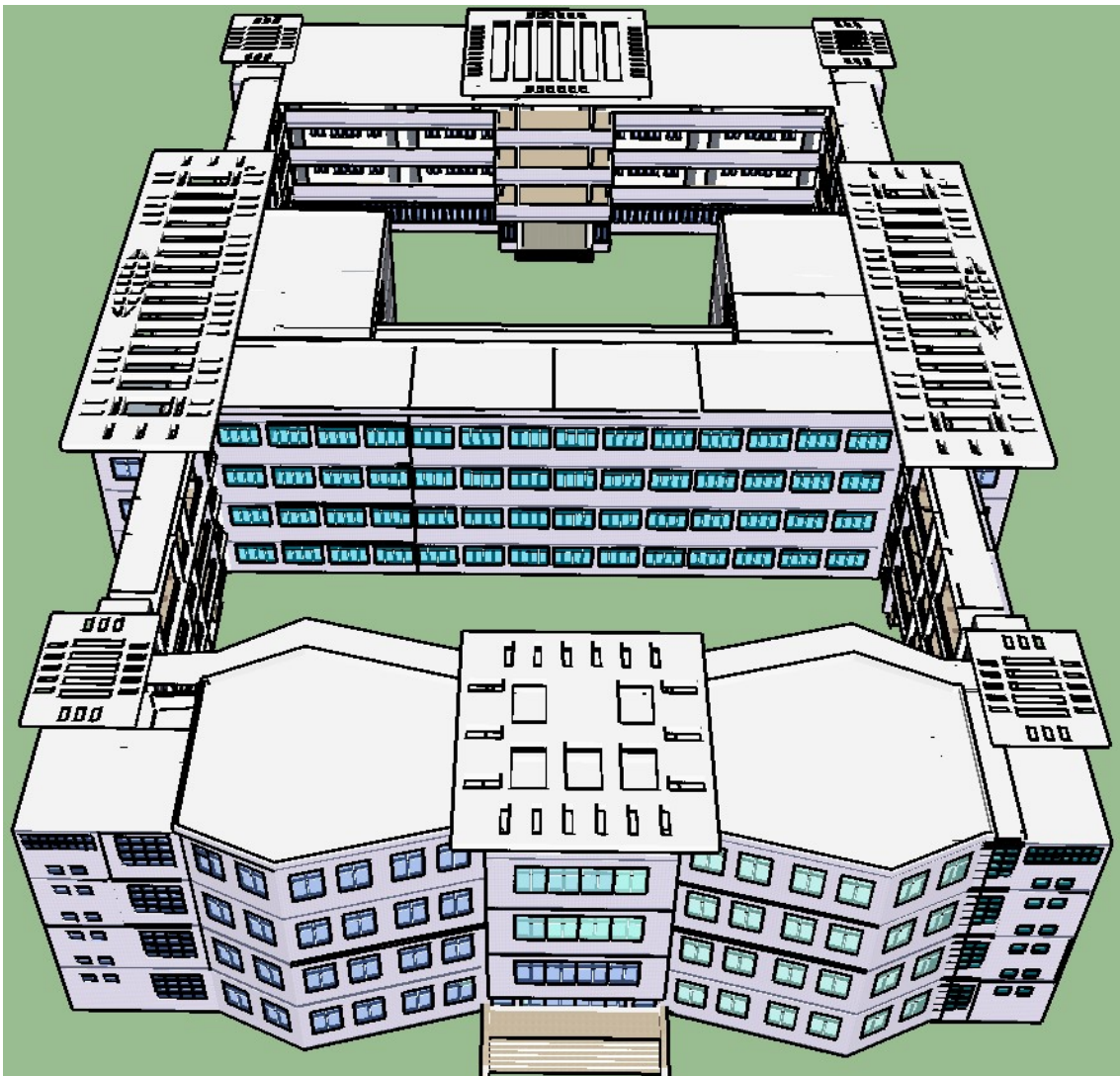


Figure 3. South view of the 3D model for the Henan University of Urban Construction (HUUC) building.



Figure 4. A graphic demonstration of the 3D model for the Meiluocheng (MLC) building.

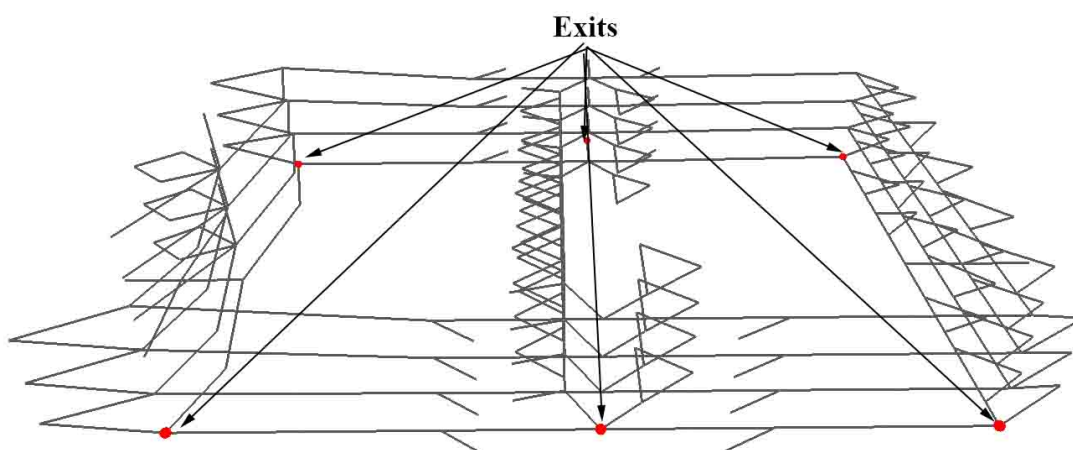


Figure 5. East view of the navigation graph for the HUUC building.

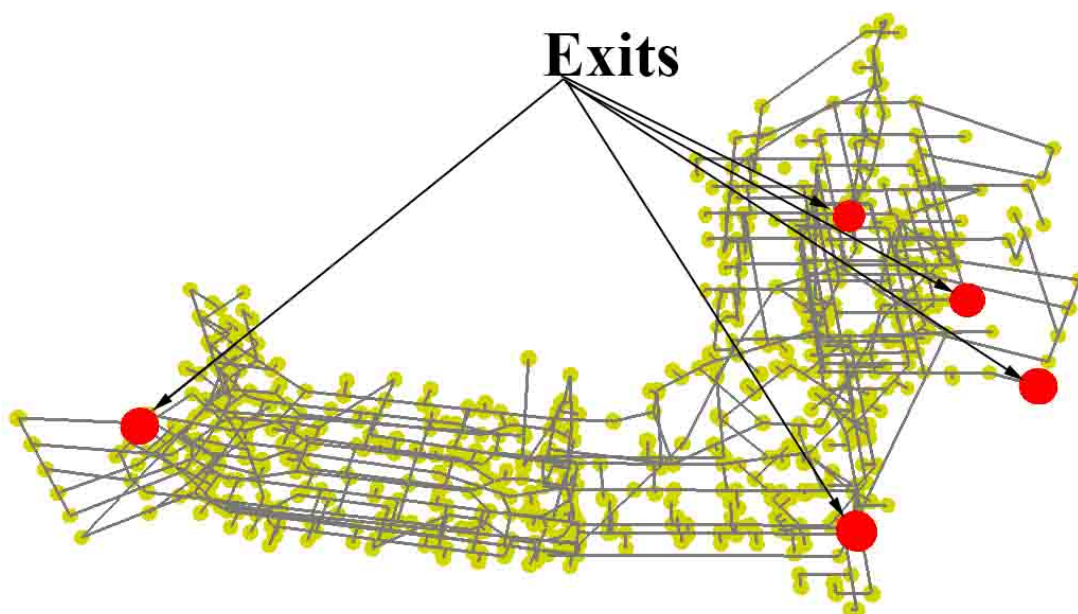


Figure 6. Navigation network demonstration for the MLC building.

3.6. Experimental Configuration

We aim to introduce four new characteristic indices for the studied navigation graph: the number of edges outside the 3D covering ball formed by using SD as the radius and the current node as the center, the number of edges inside this ball, the sum of the nodes outside this ball, and the sum of the nodes inside this ball. These four indices illustrate the edge weights compared with SD and the node quantity relative to the average length, and they show the experimental navigation graph's spatial distribution features. In addition to the above indices, we provide additional IDs to identify multiple pathfinding results for the two experimental buildings. We use these IDs with the four levels of nodes searching percentage to design the main practical scheme, which we use to demonstrate the search time efficiency and egress path quality achieved by considering the 3D evacuation network's spatial weights.

4. Experimental Results

4.1. Existing Index Analysis of the Studied Buildings

We generate the attribute values of the experimental buildings in Table 3 and the classical values according to the existing methods (we describe these methods in detail across Duan's and Porta's studies [19,24]). The first two lines of this table illustrate networks with comparatively low ratios between nodes and edges. The gamma index shows that these two networks have smaller numbers of edges than a fully connected system based on the same number of nodes. The transitivity values of these two networks are quite different. The value is over 0.2 for the HUUC building, but for the MLC building, the amount is quite small (less than 0.0041). This transitivity value difference means that the former building can connect the neighbor nodes more than the latter building. The average path length (L_{aop}) describes that there are less than ten nodes for the ordinary path across the entire network for the HUUC building, and this means that its L_{aop} is short; this value for the MLC building is over 20 nodes, which means that its L_{aop} is long. The graph diameter here depicts the longest path distance covering more than 200 nodes, and it is a significantly large value for the MLC building. The local connectivity (C_l) for the HUUC building is approximately 0.8, and for the MLC building, it is approximately 0.7; both of these values are less than 1. These local connectivity values mean that the average influence of removing a single node is minimal. In other words, removing any node may not affect the primary network structure. Interestingly, the above features generated by the traditional network analysis method counter common sense for navigation analysis purposes. Although building exits' spatial distribution significantly affects evacuation efficiency, many traditional network features ignore this phenomenon, whereas our proposed method reflects this exit neighboring phenomenon.

Table 3. Index and attribute values of the navigation graphs for the experimental buildings.

Index Name	HUUC	MLC	Unit
Number of Nodes	256	841	N/A
Number of edges	324	943	N/A
Gamma index	0.009926	0.002669	N/A
Transitivity	0.2006221	0.004065041	N/A
Average node path length	9.834926	20.803516	Nodes
Graph diameter	20	202.824722	Nodes
Local connectivity	0.8203	0.7063	N/A
Average spatial distance (SD)	4.22410244	3.349026	Metre
Number of edges with distance larger than SD	54	266	N/A
Number of edges with distance smaller than SD	270	677	N/A
Number of nodes with distance larger than SD	254	839	N/A
Number of nodes with distance smaller than SD (Q)	2	2	N/A

Figures 7 and 8 show spatial views and statistical views, which we generate by combining the last four rows of Table 3, to supplement the spatial relationships beyond the pure graph feature view. As shown in Figures 7 and 8, these 3D scenes demonstrate the average distances between the values in the row “average spatial distance (SD)”, which we generate by calculating the arithmetic averages of the SD s for the whole navigation network, of Table 3 and the actual spatial distributions of the nodes and edges. We can perceive that most MLC and HUUC buildings’ nodes only cover the nearest neighbors within SD . This situation continues for edges in the HUUC building, which is proven by less than 20% of its edges shorter than SD . However, nearly one-third of the edges in the MLC building are more extended than SD .

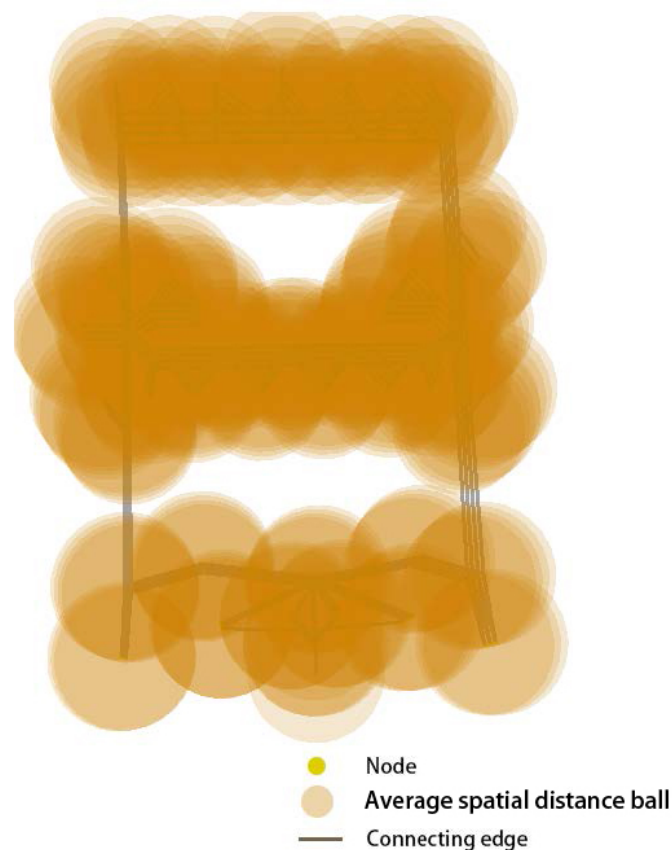


Figure 7. The scope of the average node spatial distance for the HUUC building.

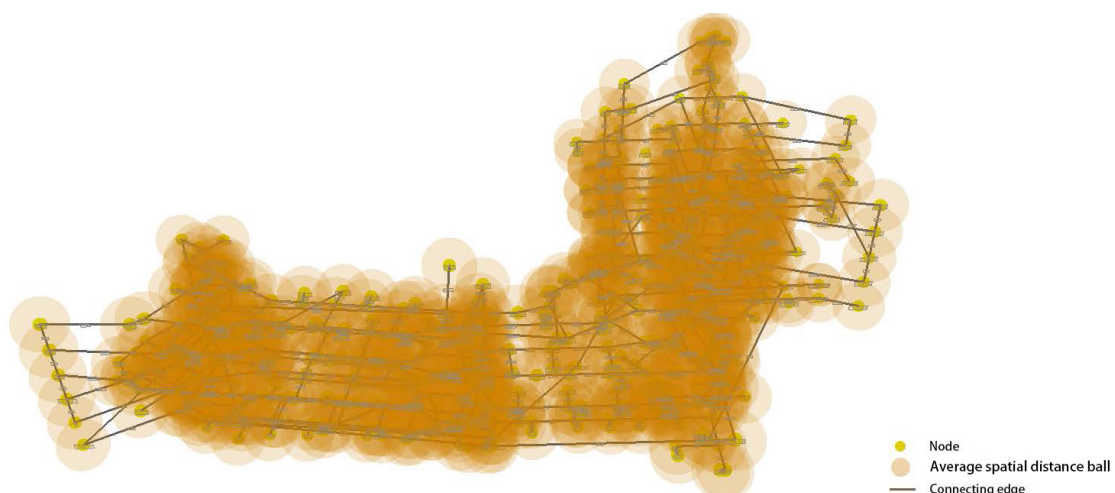


Figure 8. The scope of the average node spatial distance for the MLC building.

4.2. Proposed Spatial Index Analysis of the Studied Buildings

Table 4 summarizes the results from the studied buildings' calculation using the proposed indices. We provide bar plots for the numbers of valid paths in the experiment buildings (C_m) (Figure 9), and we observe that this number is significant for the MLC building—over 600 under most circumstances. The meaningful result values for the HUUC building are slightly small because fire events can significantly hinder the indoor navigation network's overall connectivity status compared to that of the MLC building under the same spatial setting. In Figure 10, the SD values between nodes and exits for various tests are quite different. Under most circumstances, the typical SD s are below 10 m for both buildings; however, this is not the case for the classical evacuation path generation. For both structures, the traditional process of searching through all nodes generates comparatively large SD s, and this situation also appears in the row "spatial sorted/node path/first percentage search" of Table 4. We can attribute the former case to the ignorance of the spatial weights in the path generation process. This ignorance leads to a significant increase in the SD of the MLC building to approximately 40 m and a similar increase of around 10 m in the HUUC building. We can explain the latter increase by the ignorance of the spatial weights during the pathfinding process when we only consider node distances; the choice of a smaller number of nodes along the egress path that crosses the fire disaster regions thus leads to a significant increase in the spatial weights along the generated egress path. We can explain that this situation does not appear for other settings of the node usage percentage as follows: the 20%, 50%, and 80% settings in the fourth column of Table 3 are sufficiently large to allow the pathfinding process to take comparatively safe and short node paths to egress; thus, the pathfinding process cannot receive prominent benefits by increasing the searching scope.

Table 4. Indices and attribute values of the navigation graphs for the studied buildings.

ID	Search Option	Experiment Area	Percentage of Using Nodes
AA	Classical method/node search	MLC	100%
AB	Classical method/spatial search	MLC	100%
AC	Spatial sorted/node path/first percentage search	MLC	10%
AD	Spatial sorted/spatial path/first percentage search	MLC	10%
AE	Node sorted/node path/first percentage search	MLC	10%
AF	Node sorted/spatial path/first percentage search	MLC	10%
AG	Spatial sorted/node path/second percentage search	MLC	20%
AH	Spatial sorted/spatial path/second percentage search	MLC	20%
AI	Node sorted/node path/second percentage search	MLC	20%
AJ	Node sorted/spatial path/second percentage search	MLC	20%
AK	Spatial sorted/node path/third percentage search	MLC	50%
AL	Spatial sorted/spatial path/third percentage search	MLC	50%
AM	Node sorted/node path/third percentage search	MLC	50%
AN	Node sorted/spatial path/third percentage search	MLC	50%
AO	Spatial sorted/node path/fourth percentage search	MLC	80%
AP	Spatial sorted/spatial path/fourth percentage search	MLC	80%
AQ	Node sorted/node path/fourth percentage search	MLC	80%
AR	Node sorted/spatial path/fourth percentage search	MLC	80%
AS	Classical method/node search	HUUC	100%
AT	Classical method/spatial search	HUUC	100%
AU	Spatial sorted/node path/first percentage search	HUUC	10%
AV	Spatial sorted/spatial path/first percentage search	HUUC	10%
AW	Node sorted/node path/first percentage search	HUUC	10%
AX	Node sorted/spatial path/first percentage search	HUUC	10%
AY	Spatial sorted/node path/second percentage search	HUUC	20%
AZ	Spatial sorted/spatial path/second percentage search	HUUC	20%
BA	Node sorted/node path/second percentage search	HUUC	20%
BB	Node sorted/spatial path/second percentage search	HUUC	20%
BC	Spatial sorted/node path/third percentage search	HUUC	50%
BD	Node sorted/node path/third percentage search	HUUC	50%
BE	Spatial sorted/spatial path/third percentage search	HUUC	50%
BF	Node sorted/spatial path/third percentage search	HUUC	50%
BG	Spatial sorted/node path/fourth percentage search	HUUC	80%
BH	Spatial sorted/spatial path/forth percentage search	HUUC	80%
BI	Node sorted/node path/fourth percentage search	HUUC	80%
BJ	Node sorted/spatial path/fourth percentage search	HUUC	80%

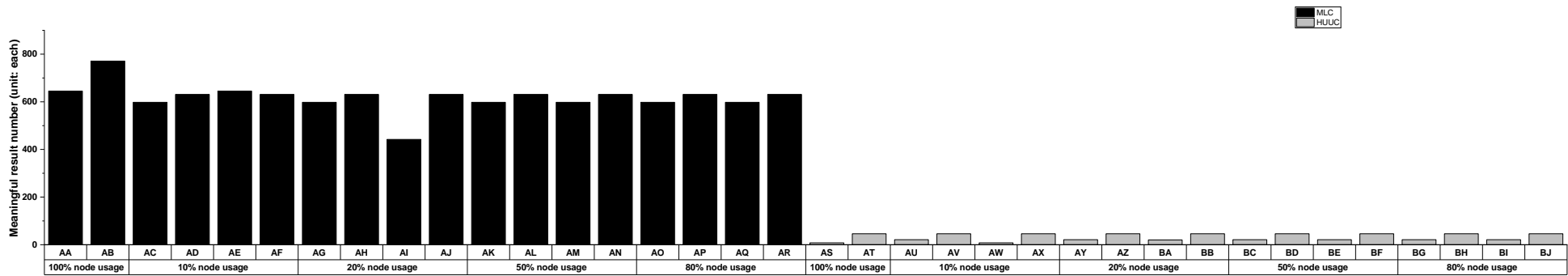


Figure 9. Numbers of valid paths for two studied buildings with different percentage settings of using nodes.

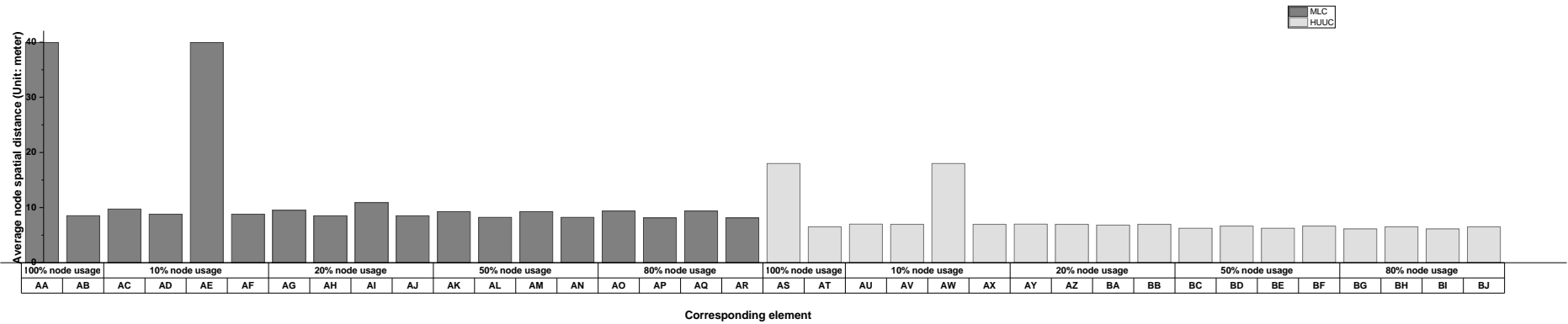


Figure 10. Average spatial distance values for two studied buildings with different percentage settings of using nodes.

In Figure 11, the average time costs (T_{aop}) for the HUUC building under different circumstances follow the trend that a search time increase accompanies the percentage setting increase, and the search time achieved while considering the spatial weights is shorter than that yielded by finding the spatial influences under nodes sorted without considering the spatial weights. Nevertheless, the node sorting process that utilizes the spatial weights alters this trend. The situation compensates this benefit that the time cost of obtaining results while considering the spatial weights is still higher than that of getting the results without considering the spatial weights; the time cost decreases with the first, second, and third percentage settings but not with the fourth percentage setting. We may attribute this phenomenon to the small total number of nodes in the HUUC building, and the spread of the fire almost paralyzes the central part of its whole navigation network. Therefore, under the first three percentage settings, the pathfinding process stops at an early search stage, and the search time thus decreases. When the node search percentage is 80%, the pathfinding program can generate an egress path, and the time cost increases. The situation in Figure 12 is quite different from that in Figure 11. For the MLC building, the average time cost continually increases as the percentage of nodes used increases and the introduction of spatial weights during the node sorting process. A few exceptions appear: the time cost of the third percentage setting for node sorting without introducing spatial weights is slightly shorter than that of the other percentage settings. We attribute this to the percentage increase from 20% to 50%, which helps the pathfinding program bypass the fire influence regions and thus leads to a slight rise in time spent. For the long-term high cost of the first percentage setting with the node sorting method including spatial weights, the reason for this occurrence could be that the 10% node selection setting is inefficient for the pathfinding program to generate available egress paths and causes a significant time increase compared to other settings.

In Figure 13, the *SDs* of the methods considering the different percentages of nodes used are almost the same as expected: the usage of the node sorting method significantly reduces the average spatial distance for the generated path. Only one exception appears: the non-sorted classical result for the HUUC building is shorter than the result obtained with the first percentage setting. This exception can attribute to the limited number of nodes in this building. Therefore, when a fire spreads, only a few nodes are available for pathfinding. The number of possible egress paths is limited; thus, classical methods that only consider node paths can still generate a spatial distance-optimized result. Figure 14 shows the reduction ratio of the path result distance between the generated node-centered path and the spatial-centered path. We observe that the reduction ratio is small across all the HUUC building results, except the classical method and the first percentage setting considering the node sorting process's spatial weights. We can explain this exception by the small number of nodes in the HUUC building; thus, the pathfinding program produces the spatial weight-centered path without considering the spatial weight element. However, the reduction ratio case for the MLC building is different: the reduction ratios for all situations are easily perceived. The reduction ratio is significant when the spatial path distance generated by nonspatial weight methods is also long, and this ratio is small when the *SD* is short.

Generally, illustrations from a graph perspective demonstrate the connectivity features of the main network structure but may contradict a real building-based navigation network's spatial distribution. Nonetheless, we can mitigate this gap by introducing spatial weights. Moreover, we observe that navigation networks' spatial views can show the spatial distribution trends of the experimental buildings and network connectivities. Additional spatial elements, such as the spatial intensities of nodes and edges in navigation networks, can be introduced into the graph analysis in future work.

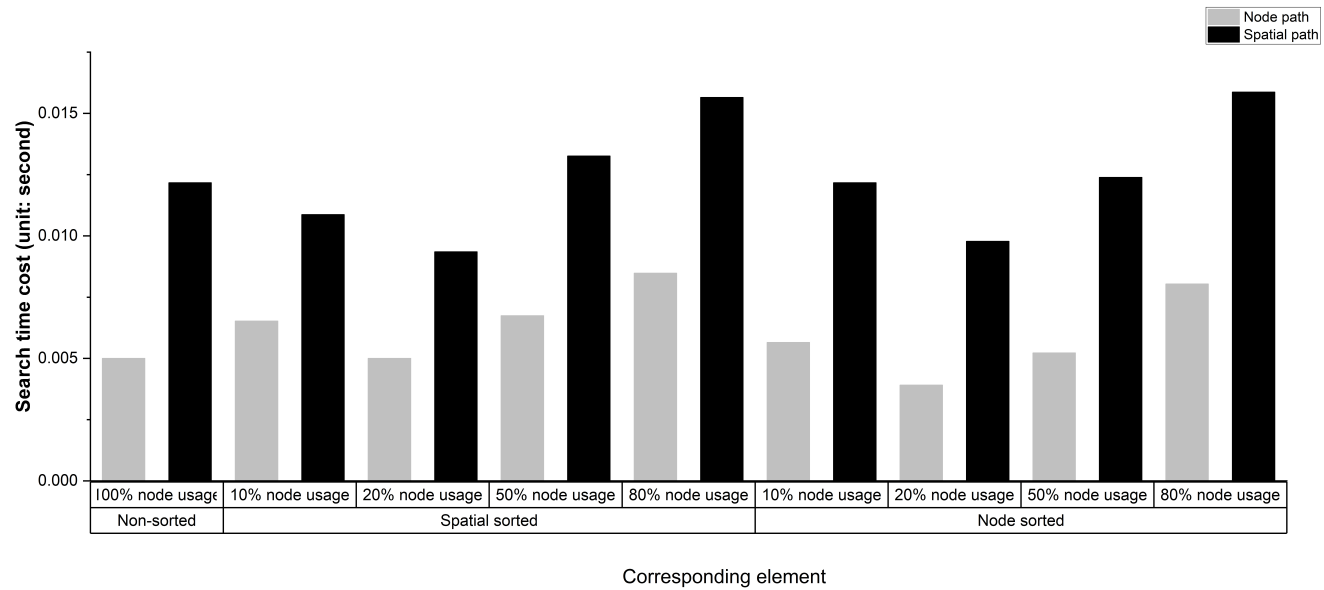


Figure 11. The search time costs of the HUUC building with different node usage percentage settings.

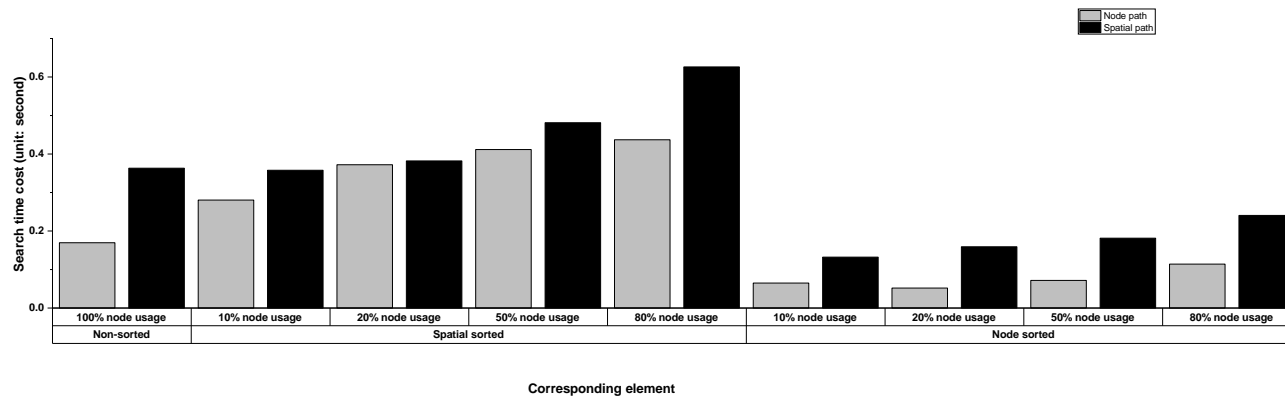


Figure 12. The search time costs of the MLC building with different node usage percentage settings.

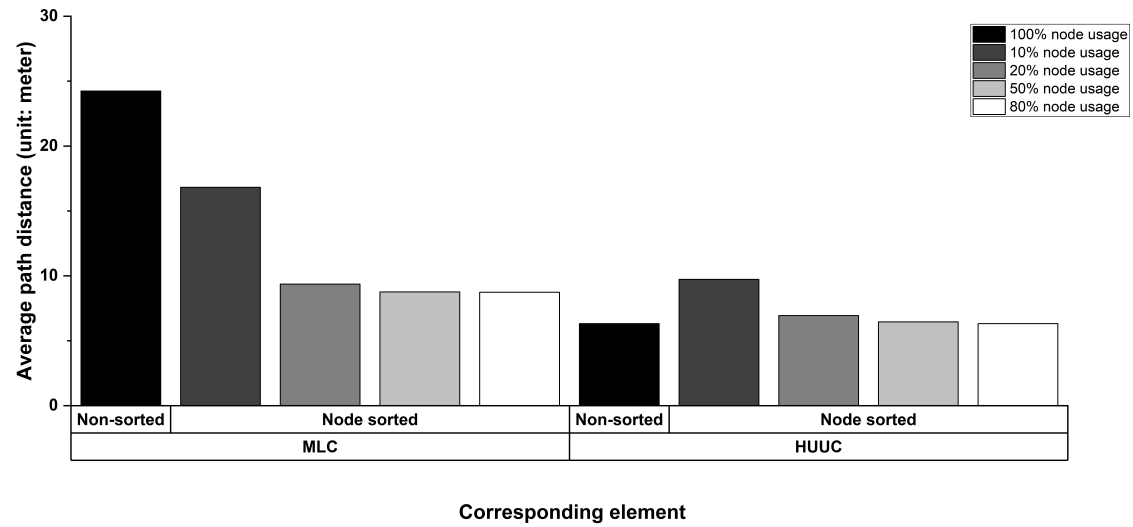


Figure 13. Average path spatial distances of the two studied buildings with different node usage percentage settings.

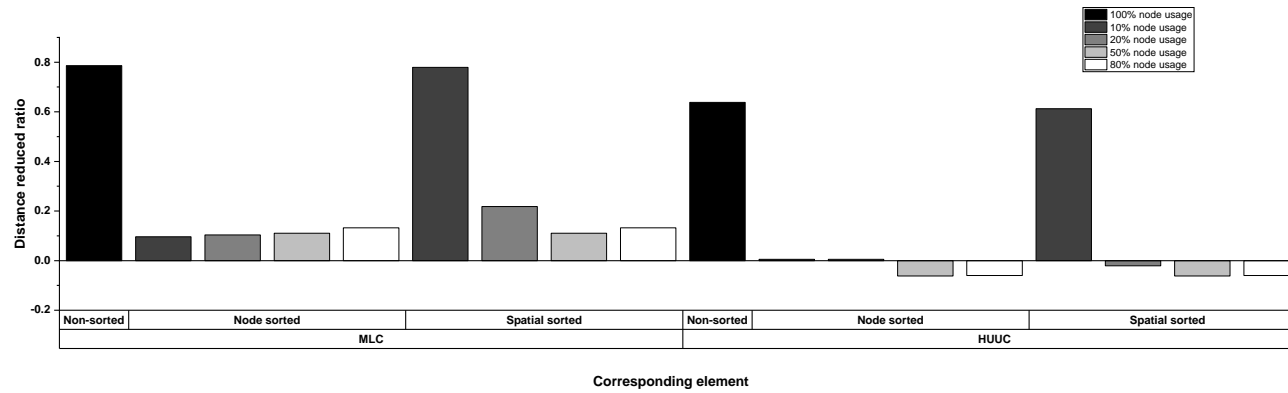


Figure 14. Distance reduction ratios of the two studied buildings with different node usage percentage settings.

5. Conclusions and Future Works

In this paper, we have proposed a method to evaluate indoor navigation networks' connectivity for emergency evacuations. We have defined a set of indices to describe navigation networks' statuses during disasters from the graph view and the spatial metric perspective. In this method, we use both the 3D geometric distance measure and the fire spread model, and this allows us to estimate the fires' influences on the neighboring clusters of accessible nodes in the 3D network. We can link the isolated groups of accessible nodes through the spatial sorting of nodes, facilitating the process of generating and selecting the minimum-risk evacuation paths and reducing the search time cost.

We suggest several directions for future research: First, currently, a simple fire model is used in this paper to estimate the influence of fires on indoor networks. The model breaks down the continuous fire spreading process into discrete steps and assumes that the fire spreads with a static speed in all directions. In the next step, we can drive a more complex fire simulation model (e.g., [31]) by real-time data and better predict how fires spread to estimate the influence of fires on indoor environments. Second, heuristic routing methods such as A*, which can consider the proposed indices, will also be developed to generate feasible and safe routes in disastrous situations. Third, we will improve the definitions of the index by considering human behaviors. During emergencies, the network's connectivity status is affected by hazards and influenced by evacuees' movements, which could result in congestion at specific nodes and edges. Therefore, there is also a need to integrate the human factor in the network robustness analysis. Finally, we may apply our network robustness evaluation method to flooding and other emergency evacuation networks after a thorough investigation of the considered network features.

Author Contributions: Conceptualization, Lei Niu; methodology, Lei Niu; software, Lei Niu; validation, Zhiyong Wang; formal analysis, Zhiyong Wang; investigation, Yiquan Song; resources, Yi Li; data curation, Yiquan Song; writing—original draft preparation, Lei Niu; writing—review and editing, Lei Niu and Zhiyong Wang; visualization, Yiquan Song; supervision, Lei Niu; project administration, Zhiyong Wang; funding acquisition, Lei Niu. All authors have read and agreed to the published version of the manuscript.

Funding: This research was funded by the National Science Foundation of China (41771433, 41501440, 41571387, 41471341); Tianjin Natural Science Foundation (No.18JCYBJC90600).

Data Availability Statement: The data presented in this study are available on request from the corresponding author.

Acknowledgments: This research is supported by the data collected by Jiwei Chu and Shuqian Li.

Conflicts of Interest: The authors declare no conflict of interest. The funders had no role in the design of the study; in the collection, analyses, or interpretation of data; in the writing of the manuscript, or in the decision to publish the results.

References

1. Park, I.; Lee, J.N. Defining 3D Spatial Neighborhoods For Topological Analyses Using A 3D Network-Based Topological Data Model—Ca-Based Building Evacuation Simulation. In Proceedings of the International Society for Photogrammetry and Remote Sensing 2008 Congress, Beijing, China, 3–11 July 2008.
2. Tan, L.; Hu, M.; Lin, H. Agent-based simulation of building evacuation: Combining human behavior with predictable spatial accessibility in a fire emergency. *Inf. Sci.* **2015**, *295*, 53–66. [[CrossRef](#)]
3. Cao, S.; Song, W.; Lv, W.; Fang, Z. A multi-grid model for pedestrian evacuation in a room without visibility. *Phys. Stat. Mech. Its Appl.* **2015**, *436*, 45–61. [[CrossRef](#)]
4. Wang, Z.; Niu, L. A Data Model for Using OpenStreetMap to Integrate Indoor and Outdoor Route Planning. *Sensors* **2018**, *18*, 2100. [[CrossRef](#)] [[PubMed](#)]
5. Song, Y.; Gong, J.; Li, Y.; Cui, T.; Fang, L.; Cao, W. Crowd evacuation simulation for bioterrorism in micro-spatial environments based on virtual geographic environments. *Saf. Sci.* **2013**, *53*, 105–113. [[CrossRef](#)]
6. Wang, Z.; Zlatanova, S. Taxonomy of navigation for first responders. In *Progress in Location-Based Services*; Springer: Berlin/Heidelberg, Germany, 2013; pp. 297–315.
7. Meijers, M.; Zlatanova, S.; Pfeifer, N. 3D geoinformation indoors: Structuring for evacuation. In Proceedings of the Next Generation 3D City Models, Bonn, Germany, 21–22 June 2005.

8. Isikdag, U.; Zlatanova, S.; Underwood, J. A BIM-Oriented Model for supporting indoor navigation requirements. *Comput. Environ. Urban Syst.* **2013**, *41*, 112–123. [[CrossRef](#)]
9. Saberian, J.; Malek, M.R.; Winter, S.; Hamrah, M. A New Framework for Solving the Spatial Network Problems Based on Line Graphs. *Trans. GIS* **2014**, *18*, 767–782. [[CrossRef](#)]
10. Krūminaitė, M.; Zlatanova, S. Indoor space subdivision for indoor navigation. In Proceedings of the Sixth ACM Sigspatial International Workshop on Indoor Spatial Awareness, Dallas, TX, USA, 4 November 2014; pp. 25–31.
11. Wang, J.; Jebara, T.; Chang, S.F. Semi-supervised learning using greedy max-cut. *J. Mach. Learn. Res.* **2013**, *14*, 771–800.
12. Mao, B.; Li, B. Graph-Based 3D Building Semantic Segmentation for Sustainability Analysis. *J. Geovis. Spat. Anal.* **2020**, *4*, 1–12. [[CrossRef](#)]
13. Lee, J. A Three-Dimensional Navigable Data Model to Support Emergency Response in Microspatial Built-Environments. *Ann. Assoc. Am. Geogr.* **2007**, *97*, 512–529. [[CrossRef](#)]
14. Lee, J.; Zlatanova, S. A 3D data model and topological analyses for emergency response in urban areas. In *Geospatial Information Technology for Emergency Response*; Zlatanova, S., Li, J., Eds.; CRC Press: Boca Raton, FL, USA, 2008; pp. 143–168.
15. Lee, J. Spatial Data Analysis in 3D GIS. In *Advances in 3D Geoinformation Systems*; Springer: Berlin/Heidelberg, Germany, 2008; p. 435.
16. Tang, H.; Elalouf, A.; Levner, E.; Cheng, T. Efficient computation of evacuation routes on a three-dimensional geometric network. *Comput. Ind. Eng.* **2014**, *76*, 231–242. [[CrossRef](#)]
17. Reddy, K.U.K. A survey of the all-pairs shortest paths problem and its variants in graphs. *Acta Univ. Sapientiae Inform.* **2016**, *8*, 16–40. [[CrossRef](#)]
18. Kivelä, M.; Cambe, J.; Saramäki, J.; Karsai, M. Mapping temporal-network percolation to weighted, static event graphs. *Sci. Rep.* **2018**, *8*, 12357. [[CrossRef](#)] [[PubMed](#)]
19. Porta, S.; Crucitti, P.; Latora, V. The network analysis of urban streets: A primal approach. *Environ. Plan. Plan. Des.* **2006**, *33*, 705–725. [[CrossRef](#)]
20. Mahmassani, H.S.; Saberi, M. Urban network gridlock: Theory, characteristics, and dynamics. *Procedia Soc. Behav. Sci.* **2013**, *80*, 79–98. [[CrossRef](#)]
21. Liu, J.; Xiong, Q.; Shi, W.; Shi, X.; Wang, K. Evaluating the importance of nodes in complex networks. *Phys. A Stat. Mech. Its Appl.* **2016**, *452*, 209–219. [[CrossRef](#)]
22. Snelder, M.; Van, H.; Immers, L. A framework for robustness analysis of road networks for short term variations in supply. *Transp. Res. Part A Policy Pract.* **2012**, *46*, 828–842. [[CrossRef](#)]
23. Chen, L.; Zhang, J.; Cai, L.-J. Overlapping community detection based on link graph using distance dynamics. *Int. J. Mod. Phys. B* **2018**, *32*, 1850015. [[CrossRef](#)]
24. Duan, Y.; Lu, F. Structural robustness of city road networks based on community. *Comput. Environ. Urban Syst.* **2013**, *41*, 75–87. [[CrossRef](#)]
25. Jenelius, E.; Mattsson, L.G. Road network vulnerability analysis: Conceptualization, implementation and application. *Comput. Environ. Urban Syst.* **2015**, *49*, 136–147. [[CrossRef](#)]
26. Leskovec, J.; Lang, K.J.; Dasgupta, A.; Mahoney, M.W. Community structure in large networks: Natural cluster sizes and the absence of large well-defined clusters. *Internet Math.* **2009**, *6*, 29–123. [[CrossRef](#)]
27. Kitska, M.; Gallos, L.K.; Havlin, S.; Liljeros, F.; Muchnik, L.; Stanley, H.E.; Makse, H.A. Identifying influential spreaders in complex networks. *Nat. Phys.* **2010**, *6*, 888–893. [[CrossRef](#)]
28. Zhang, J.X.; Chen, D.B.; Dong, Q.; Zhao, Z.D. Identifying a set of influential spreaders in complex networks. *Sci. Rep.* **2016**, *6*, 27823. [[CrossRef](#)] [[PubMed](#)]
29. Pareto, V. *Manual of Political Economy*; A.M. Kelley: New York, NY, USA, 1971.
30. DiNunno, P.J. *SFPE Handbook of Fire Protection Engineering: National Fire Protection Association Quincy*; Springer: New York, NY, USA, 1988.
31. Moreno, A.; Segura, Á.; Korchi, A.; Posada, J.; Otaegui, O. Interactive urban and forest fire simulation with extinguishment support. In *Advances in 3D Geo-Information Sciences*; Springer: Berlin/Heidelberg, Germany, 2011; pp. 131–148.